The effect of wake turbulence intensity on transition in a compressor cascade

Jan G. Wissink
School of Engineering and Design, Brunel University,
Uxbridge UB8 3PH, UK
and
Tamer A. Zaki
Department of Mechanical Engineering, Imperial College,
London SW7 2AZ, UK
and
Wolfgang Rodi
Institute for Hydromechanics, University of Karlsruhe,
Kaiserstr. 12, D-76128 Karlsruhe, Germany and
King Abdulaziz University, Jeddah, Saudi Arabia
and
Paul A. Durbin
Aerospace Engineering, Iowa State University,
Iowa, USA

Abstract

Direct numerical simulations of separating flow along a section at midspan of a low-pressure V103 compressor cascade with periodically incoming wakes were performed. By varying the strength of the wake, its influence on both boundary layer separation and bypass transition were examined. Due to the presence of small-scale three-dimensional fluctuations in the wakes, the flow along the pressure surface was found to undergo bypass transition. Only in the weak-wake case, the boundary layer was found to reach a nearly-separated state between impinging wakes. In all simulations, the flow along the suction surface was found to separate. In the simulation with the strong wakes, separation was found to be intermittently suppressed as the periodically passing wakes managed to trigger turbulent spots upstream of the location of separation. As these turbulent spots were convected downstream, they locally suppress separation.

1 Introduction

Low Pressure (LP) compressors typically consist of a large number of stages. The actual increase in pressure that can be realized in each stage is limited by the need to avoid massive boundary-layer separation which affects the aerodynamic performance of the blades and may cause structural damage. To some degree, separation is controlled by free-stream fluctuations generated by the preceeding row of blades. To correctly predict the effects of impinging free-stream turbulence on the state of the blade's boundary layer, advanced modelling strategies are needed. In engineering applications a variety of models are employed to predict the state of the boundary layer [9]. These range from crude algebraic models to more complex and accurate models based on transport equations, as can be seen in [2, 10]. To improve existing models and to design new models for transition, data from both experiments and time-accurate numerical simulations are needed.

Several experiments of flow in LP turbine cascades have been performed in the past [14, 15]. The accompanying DNS-s [8, 18, 20, 21] allowed an even more detailed study of the physical mechanisms that drive boundary-layer transition in LP turbine blades. Relatively less effort has been dedicated to DNS of flow in compressor cascades. The present simulations are motivated by the experiments of flow in the LP V103A compressor cascade performed by Hilgenfeld and Pfitzner [6] who studied the combined effects of impinging wakes and background turbulence on

the development of the suction side boundary layer. It was found that the added effect of the periodically passing wakes on the blade's boundary layer was largely masked by the overall effect of the uniformly distributed isotropic background turbulence. Hence, it was not possible to accurately analyse the influence of the periodically passing wakes on separation and transition of the compressor blade's boundary layer.

Even though the available computational resources have increased significantly, a Direct Numerical Simulation (DNS) of the flow in realistic turbine or compressor stages is still far beyond the capabilities of modern supercomputers. The Reynolds number of such flows, however, is moderate, such that performing a DNS of flow for a simplified geometry - such as a two-dimensional section at midspan - is feasible. The first DNS-s of flow in a T106 turbine cascade with periodically incoming wakes were performed by Wu and Durbin [21] and Wissink [18]. In both simulations, production of fluctuating kinetic energy was observed at the apex of the deformed wake as it traveled through the passage between blades, and streamwise longitudinal vortical structures were found along the pressure side . These longitudinal structures formed as the accelerating flow adjacent to the pressure side stretched the vortical structures in the wake, thereby aligning them with the direction of flow. Removing all fluctuations from the wake (see [20]) was found to be sufficient to stop both the production of kinetic energy at the apex of the deformed wake and the formation of longitudinal structures along the pressure side of the blade. While in the simulation by Wu and Durbin [21] the suction side boundary layer was observed to undergo bypass transition, the larger inflow-angle employed in the simulation by Wissink [18] was found to lead to an intermittent separation of the boundary layer along the downstream half of the suction side. Kalitzin et al. [8] reported on a DNS of flow in the T106 turbine cascade with incoming free-stream turbulence (FST). Compared to the earlier DNS with incoming wakes by Wu and Durbin, the location of transition of the suction side boundary layer was found to move further downstream. Because of the presence of high levels of free-stream fluctuations, the boundary layer flow on an LP turbine blade usually undergoes bypass transition.

The mechanism of bypass transition has been clarified by a number of studies of canonical boundary-layer flows, see e.g. [7, 24, 25, 11]). The mean-flow shear acts as a low-pass filter by only allowing low-frequency components of the free-stream turbulence into the boundary layer [26]. These penetrating disturbances cause the amplification of elongated streaks, also known as Klebanoff modes. The streaks can reach amplitudes on the order of $10 - 30\%$ of the free-stream speed, and some undergo a secondary instability that precedes the inception of localized turbulence spots [12]. The nature of the secondary instability depends on the flow configuration, for example the pressure gradient, and can be initiated near the edge of the boundary layer on close to the wall [17, 5]. Once formed, the turbulence spots grow as they are convected in the downstream direction, and finally merge into the fully-turbulent region.

Compared to the flow around an LP turbine blade, the boundary layer flow around an LP compressor blade is more likely to separate and separation-induced transition is relatively common. Motivated by the experiments in the V103 compressor cascade [6], where it was found that the effect of the periodically impinging wakes on boundary layer transition was masked by the high intensity of the incoming background turbulence, a series of DNS-s of flow in a V103 compressor cascade was performed [22]. In these simulations the effect of FST alone (without wakes) on the blade's boundary layer was studied. In the presence of FST, the boundary layer on the pressure side was found to remain attached due to transition to turbulence upstream of the location of separation in the laminar case. Along the suction surface, the separation was found to persist even at high levels of FST. By varying the levels of the FST, a rich variety of transitional mechanisms was found along the suction surface . At moderate levels of disturbances, two-dimensional waves could be identified and their development was still influenced by Klebanoff streaks due to the free-stream forcing. For high levels of free-stream disturbances, the transition mechanism was found to shift towards a pure bypass transition scenario.

Zaki et al. [27] studied the influence of periodically incoming weak wakes on transition and compared the flow to calculations without any inflow disturbances. On the pressure surface, the wakes were found to fully suppress separation by periodically triggering bypass transition somewhat downstream of the leading edge. On the suction surface, only a periodic reduction in the size of the separation bubble was observed. The detached boundary layer was found to roll up owing to a KH instability. Inside the rolls, the production of turbulent kinetic energy resulted in the formation of a turbulent wake-like flow downstream of the separation bubble, parallel to the suction surface. It remained unclear, however, whether a stronger wake turbulence intensity can indeed suppress separation entirely or, perhaps, intermittently in the case of a strong adverse pressure gradient in the compressor passage. Whether this is the case will be examined herein using direct numerical simulations.

One study relevant to this issue is the work by Coull and Hodson [3], although they focused on the pressure distribution typical for the suction surface of a turbine blade, where the pressure gradient is locally adverse. They performed experiments of boundary layer transition on a flat plate. The curvature of the top wall induced a varying streamwise pressure gradient along the plate that closely resembles the situation on the suction side of a high-lift LP turbine blade. The varying pressure gradient resulted in boundary-layer separation in the absence of free-stream

disturbances. A detailed study was performed of how FST and periodically passing wakes affect boundary-layer tansition and separation. The grid-generated FST was found to induce weak Klebanoff streaks that, together with the KH instability of the separated boundary layer, were found to promote transition. The addition of periodically passing wakes was found to result in the generation of stronger Klebanoff streaks originating from the region near the leading edge. The amplified streaks were found to convect at speeds that are typical for turbulent spots, while the strongest disturbances were found to convect at a speed of around 70% of the free-stream velocity. Apart from the strong Klebanoff modes, the wakes also induced short span KH structures in the separated boundary layer. The combination of wake-induced streaks and KH structures was found to lead to early transition.

In the present DNS we focus on the effect of strong periodically incoming wakes (without background turbulence in between the wakes) and compare it to the results obtained in the weak-wake simulation by Zaki et al. [27]. The aim of these simulations is to elucidate the complex interaction of periodically passing wakes of various strength in a compressor cascade where the boundary layers along both the suction surface and the pressure surface are prone to separation.

2 Simulation setup

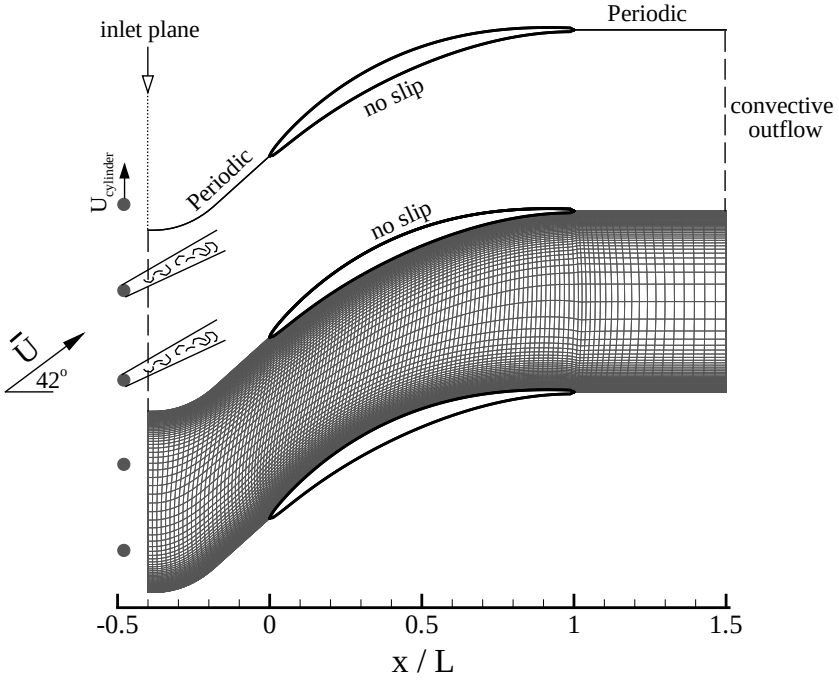

Figure 1: Upper part: Cross section through the computational domain at midspan. Lower part: Computational grid, showing every 8^{th} line in x and y

A schematic of the computational domain is shown in figure 1. In the experimental setup, the incoming wakes are generated at the inlet by vertically moving cylinders with speed $U_{cyl} = 0.30\bar{U}$. Periodic boundary conditions were employed in the spanwise direction and in the vertical direction both upstream and downstream of the compressor blade. Along the surface of the compressor blade, no-slip boundary conditions were enforced. At the outflow plane - located at $x/L = 1.5L$ - a convective outflow boundary condition was used. Finally, at the inflow plane, a uniform inflow $(u, v, w) = \bar{U}(\cos 42^o, \sin 42^o, 0)$ was prescribed on which realistic wake data (containing near-wake effects) were superimposed. The wake-data originated from a separate DNS performed by Wissink and Rodi [19] of flow around a circular cylinder at $Re_D = 3300$ (Re_D is based on the free-stream velocity and cylinder diameter D) and corresponds to a series of snapshots of the fluctuating velocity field in the plane $x = 6D$. The Reynolds number of the compressor flow problem based on the inflow velocity, $\bar{U}$, and the axial chord length, L, is $Re = 138\,500$. The pitch between blades is $P = 0.5953L$, while the distance between the vertically moving cylinders is $d_{cyl} = P/2$. The reduced frequency is

Simulation	WD	b	$Tu_{x/L=0}(\%)$	l_z
W1	$0.14U_0$	$0.0065L$	3.6	0.15L
W2	$0.16U_0$	$0.0122L$	6.0	0.15L

Table 1: Overview of the direct numerical simulations performed. WD corresponds to the maximum mean wake velocity-deficit at the inflow plane, b is the wake half-width at the location where the wake-deficit is at 50%WD L is the axial chord-length, $Tu_{x/L=0}$ is the maximum turbulence level (in the wake) at $x/L = 0$. See [27] for a detailed description of the results obtained in Simulation W1, please note that in that paper the wake half-width b is defined differently and corresponds to the half-width at the inflow plane.

$f_{red} = \frac{U_{cyl}}{d_{cyl}} \times \frac{C}{U_{exit}} = 1.40$, where C is the chord and U_{exit} is the exit velocity, the flow coefficient is $\frac{U_{exit}}{U_{cyl}} = 2.48$ and the wake velocity ratio is $\frac{U_{inlet,rel}}{U_{exit,rel}} = 0.809$, where $U_{inlet,rel}$ and $U_{exit,rel}$ are the relative velocities (in the frame of reference of the moving cylinders) at the inlet and exit, respectively.

An overview of the simulations performed is given in table 1. The wakes used in both simulations W1 and W2 correspond to scaled versions of the wake that was generated in a precursor simulation by Wissink and Rodi [19] of flow around a circular cylinder at $Re_D = 3,300$. A time-sequence consisting of 1057 snapshots of the instantaneous flow field in a vertical plane at a distance 6D behind the cylinder was stored. The series of snapshots was made periodic using a special filtering technique in order to obtain a smooth transition between the final and the first snapshots, see [19] and [27] for a more detailed description. In simulation W2, the cylinder wake is used without any rescaling. In W1 (studied in [27]), the wake is rescaled to reduce the turbulence intensity from 6% to 3.6%. In this case, the wake width is also reduced. The results obtained without wakes were reported in earlier studies [27, 22].

The simulations were performed using a finite-volume code with a collocated variable arrangement in which second-order central discretisations in space were combined with a three-stage Runge-Kutta method for the time integration. To avoid decoupling of the velocity and the pressure fields, the momentum interpolation technique of [13] was employed. The Poisson equation for the pressure was solved using the strongly implicit SIP solver [16]. A more detailed description of the numerical code can be found in [1]. To resolve the flow field, in the fully three-dimensional simulations W1 and W2, a $1030 \times 646 \times 128$ mesh was employed in the streamwise, wall-normal and spanwise directions respectively. The mesh is illustrated in figure 1 (lower part), which shows every eighth grid line of the computational mesh at mid span. Based on the experience from previous simulations, the wall-normal refinement of the computational mesh was chosen such that the grid resolution at the blade surface in wall-units was $5 < \Delta_t^+ < 10$, $0.5 < \Delta_n^+ < 1$, and $5 < \Delta_z^+ < 10$, in the tangential, normal and spanwise directions, respectively. A further verification of the accuracy of the simulations presented here can be found in [27].

To compute statistical averages, the flow through the compressor cascade was simulated for ten wake-passing periods. To improve the quality of the statistics, averaging of quantities in time and phase was combined with spatial averaging in the homogeneous spanwise direction. For the phase-averaging, each period was divided into 240 equal phases and averages $\langle f \rangle(\varphi)$ of f were gathered at each individual phase $\varphi = 0, \frac{1}{240}, \ldots, \frac{239}{240}$.

The phase-averaged turbulent kinetic energy $\langle k \rangle$ from simulation W2 is shown in figure 2 for 4 phases $\phi = \{0, 2/8, 4/8, 6/8\}$. The increased levels of $\langle k \rangle$ identify the path of the incoming wakes as they migrate through the compressor passage. In the inflow region, upstream of the leading edge of the blades, the upward moving wakes remain virtually straight. In the passage between blades, the wakes are slightly bent downwards by a moderate stretching/straining action of the mean flow. Because of this bending, the wakes impinge onto the suction side boundary layer at non-zero angle of attack. Compared with the passing wakes in the T106 turbine cascade simulations [21] and [18], where production of turbulent kinetic energy was observed at the apex of the severely deformed wakes, in the compressor passage - because of the significantly reduced turning and wake-distortion - no significant production of $\langle k \rangle$ is observed. Only along the suction surface, immediately upstream of the trailing edge, an increased production of kinetic energy is seen which is reflected by a local augmentation of $\langle k \rangle$ and indicates that the boundary layer underwent transition to turbulence.

Figure 3 compares the phase-averaged turbulence levels $\langle Tu \rangle$ at mid pitch from simulations W1 and W2 at eight phases $\phi = \{0, 1/8, 2/8, \ldots, 7/8\}$. The local maxima in Tu identify the approximate location of the axis of the wakes as they are convected by the free-stream flow through the passage between blades. As expected, the convection speed of wakes in the two simulations is the same. The difference in intensity of the wakes in the passage between blades is a direct reflection of the difference in intensity at the inflow plane.

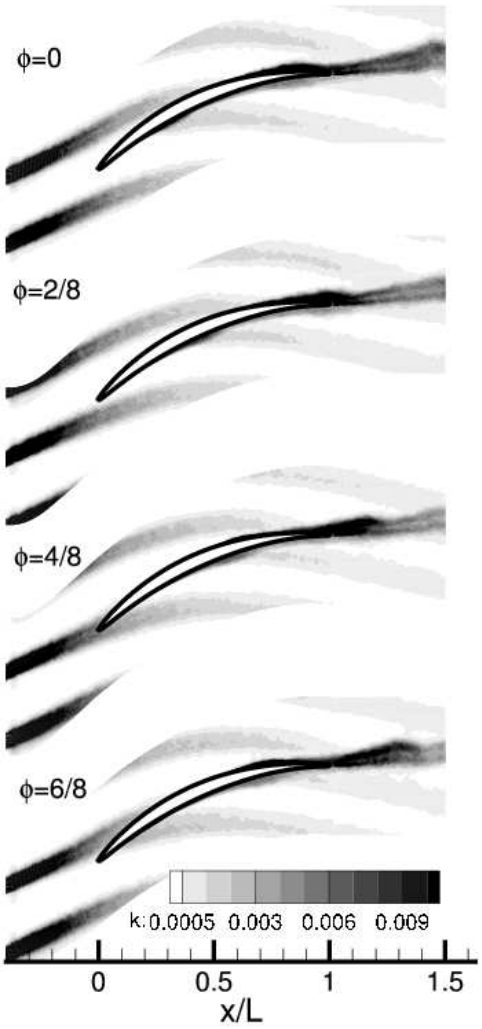

Figure 2: Simulation W2: Contours of the phase-averaged turbulent kinetic energy at 4 phases $\phi = 0, \frac{2}{8}, \frac{4}{8}, \frac{6}{8}$.

3 Time-averaged results

The evolution of the mean turbulent kinetic energy, k, along the centreline of the passage between blades is shown in figure 4. It can be seen that, in both simulations W1 and W2, k is continuously decreasing. The actual difference in both the width of the wakes and the turbulence level of the fluctuations carried by the wakes is reflected in the turbulent kinetic energy level, which in W2 is consistently about twice as high as in W1.

A comparison of the wall-static pressure coefficient C_p from simulations W1 and W2 is reported in figure 5. For both simulations, the C_p distribution along the pressure surface is found to be in good agreement. Upstream of $x/L \approx 0.8$ the streamwise pressure gradient is slightly adverse and downstream of $x/L \approx 0.8$ it becomes strongly favourable. The absence of kinks in the C_p distribution along the pressure side indicates that the boundary layer along the pressure surface remains attached in both simulations. Along the suction side, moving from the leading edge to the trailing edge, the pressure gradient is initially strongly favourable until $x/L \approx 0.2$, where it turns strongly adverse. In W1, the C_p distribution shows a clear kink between $x/L = 0.60$ and $x/L = 0.75$ - identified by the arrow - which is an indication that the flow along the suction surface separates. Towards the trailing edge, the C_p curve of simulation W1 converges to the curve from W2. In simulation W2 there is only a very weak kink in the C_p distribution along the suction surface which might indicate a mild separation region or an intermittent separation that is masked by the

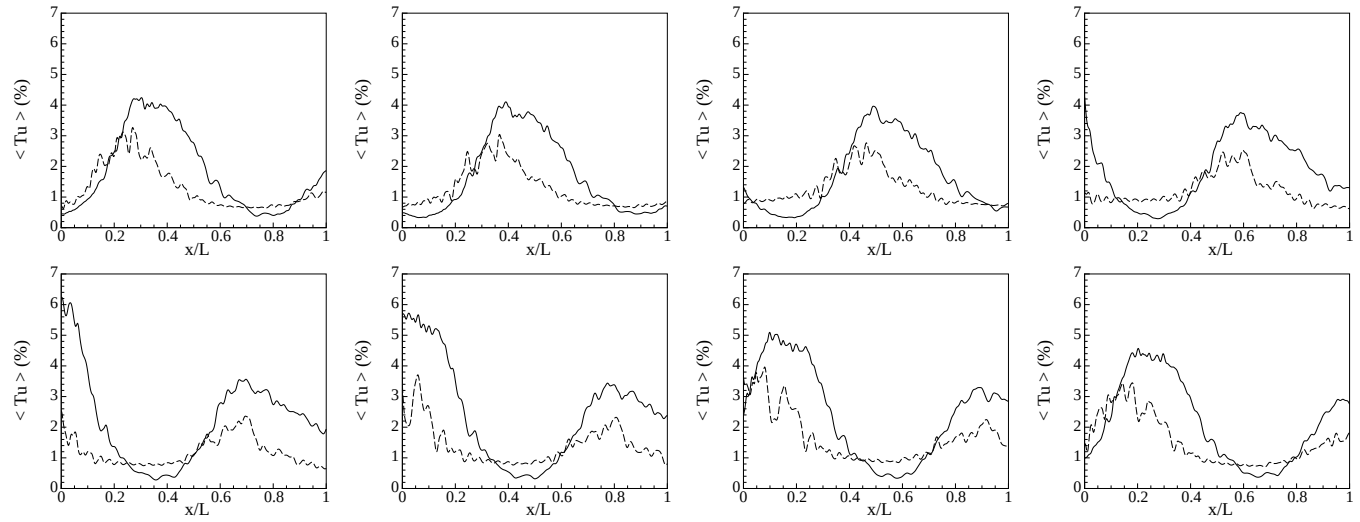

Figure 3: Phase-averaged turbulent intensity at mid-pitch at eight phases, $\phi = 0, 1/8, 2/8, \ldots, 7/8$. Comparison of simulation W2 (——) with simulation W1 (- - -) with lower intensity wakes

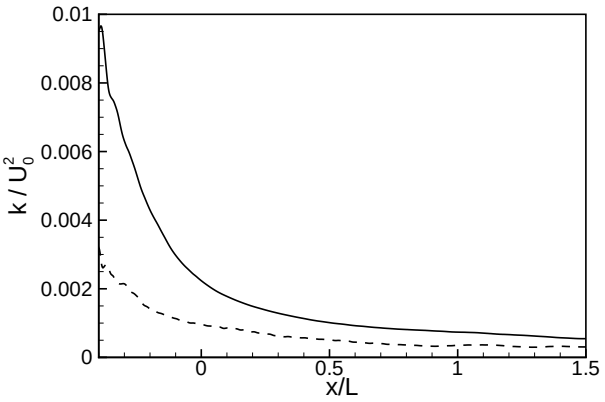

Figure 4: Time-averaged turbulent kinetic energy along the centre line of the computational domain. Simulations W1 (- - -) and W2 (——)

average across all phases. In both simulations W1 and W2, the three-dimensional free-stream turbulence in the wake manages to limit the effects of separation thereby avoiding the appearance of large coherent two-dimensional vortical structures (see Zaki et al. [22]) that would severely affect the aerodynamical properties of the blade.

The negative values of the time-averaged skin friction, C_f, along the suction surface - shown in figure 6 (left pane) - confirm that the suction side boundary layer in simulation W1 separates in the adverse pressure-gradient region between $x/L = 0.40$ and $x/L = 0.75$. Also in simulation W2 a small region around $x/L = 0.58$ exists where the boundary layer is separated. In both simulations W1 and W2, the local minimum of C_f - identifying the approximate location of the centre of the recirculation zone of the separation bubble - is followed by a rapid increase indicating that the separated boundary layer underwent transition and is reattaching as a turbulent boundary layer. While in simulation W1 this reattachment takes place between $x/L = 0.70$ and $x/L = 0.80$, in simulation W2 it is located further upstream between $x/L = 0.60$ and $x/L = 0.75$.

The time-averaged friction coefficient along the pressure surface is shown in Figure 6 (right pane). It can be seen that in both simulations W1 and W2 the time-averaged flow remains attached. The periodically impinging free-stream fluctuations in the wakes manage to trigger transition to turbulence in the decelerating boundary layer flow along the pressure surface of the blade. The onset of transition in the weak-wake simulation, W1, is located at $x/L \approx 0.22$, while

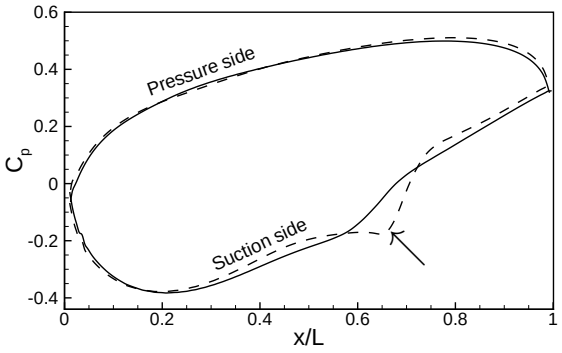

Figure 5: Time-averaged pressure coefficient around the blade surface. Comparison of simulation W2 (——) with simulation W1 (- - -) with lower intensity wakes

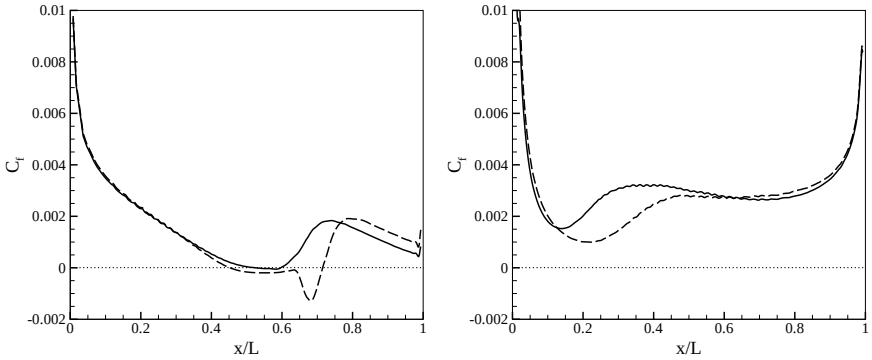

Figure 6: Time-averaged skin friction coefficient around the suction surface (left pane) and the pressure surface (right pane). Comparison of simulation W2 (——) with simulation W1 (- - -) - with lower intensity wakes

in the strong-wake simulation, W2, the onset of transition is located at $x/L \approx 0.13$. The sharp increase in the friction coefficient near the trailing edge, observed in both simulations, reflects a significant thinning of the boundary layer owing to the fact that the streamwise pressure gradient has turned strongly favourable which results in a significant acceleration of the boundary layer flow.

Figure 7 shows the time-averaged shape factor, h_{12}, from simulations W1 and W2 along the suction (left pane) and pressure surfaces (right pane), respectively. Along the suction surface, moving from the leading edge downstream, initially the shape factors in both simulations are identical and assume values that are typical for a laminar boundary layer. As the external flow decelerates, the shape factors slowly increase. Downstream of $x/L \approx 0.4$ the mean flow separation in W1 causes the shape factor to grow significantly to a maximum of $h_{12} \approx 7.5$ at $x/L \approx 0.65$. In simulation W2 the boundary layer separation is reduced, which is reflected by a significantly less pronounced growth in the shape factor and a maximum ($h_{12} \approx 4$ at $x/L \approx 0.55$) that is reached earlier than in W1. Downstream of the maximum, in both simulations the separated flow becomes turbulent and reattaches as a turbulent boundary layer with a shape-factor below 2. Along the pressure surface (right pane) again the shape factors in both simulations coincide at the leading edge having values typical for a laminar boundary layer. After a short period of initial growth, in both simulations the shape factors start to decrease to values well below $h_{12} = 2$ as the boundary layer flow undergoes transition to turbulence. Owing to the increased wake-turbulence level, in simulation W2 the transition happens sligthly earlier than in W1.

The Reynolds number, $Re_\theta = \frac{\bar{U}\theta}{\nu}$, based on the momentum thickness θ and the mean free-stream velocity $\bar{U}$, is reported in figure 8. Along the suction surface (left pane) in both simulations - moving from the leading edge downstream - the developing laminar boundary layer gives rise to a gradual growth of Re_θ. As Re_θ exceeds the value of 180 the boundary layer becomes unstable before the laminar separation point located at $x_s \approx 0.43L$ (see [27, 22]). The clear kink in the profile of W1 indicates that the free-stream fluctuations in W1 are too weak to significantly

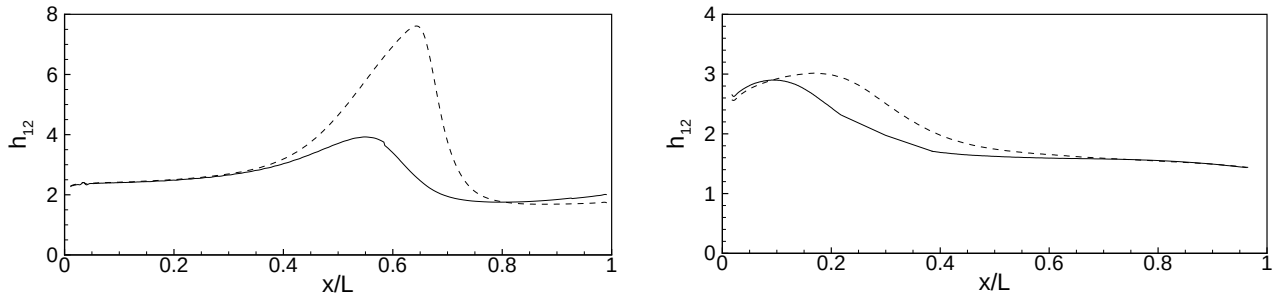

Figure 7: Time-averaged shape factor along the suction surface (left pane) and the pressure surface (right pane). Simulations W1 (- - -) and W2 (——)

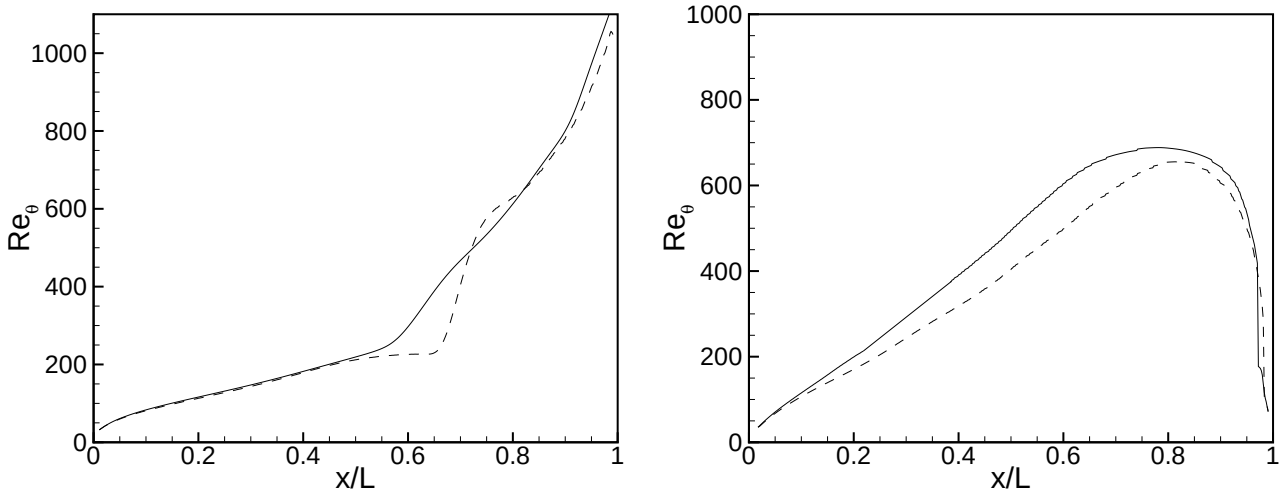

Figure 8: Time-averaged Re_θ along the suction surface (left pane) and the pressure surface (right pane). Simulations W1 (- - -) and W2 (——)

suppress separation, while the smoother behaviour of Re_θ in W2 indicates that the free-stream fluctuations manage to significantly perturb the boundary layer thereby suppressing downstream separation. Further downstream in both simulations the boundary layer becomes fully turbulent and Re_θ steadily grows until it reaches values above $Re_\theta = 1000$ near the trailing edge.

Along the pressure side (figure 8, right pane), immediately downstream of the leading edge the Re_θ-values in both simulations follow a similar trend. Once the boundary layer becomes unstable, however, in simulation W2 -with stronger disturbances - Re_θ increases faster than in W1. This reflects the fact that the laminar-to-turbulent transition in simulation W2 is established earlier than in W1. As can be seen from the C_f curve (figure Cf, right pane), transition is completed at $x/L \approx 0.45$ and 0.35 for W1 and W2, respectively. In both simulations, this corresponds to $Re_\theta \approx 350$.

4 Phase-averaged and instantaneous results

4.1 The pressure surface

The transition mechanism on the pressure surface is examined in this section. The phase dependence of transition to turbulence and the change in the boundary layer between wakes are assessed. The transition mechanism is compared to the canonical description of bypass transition, namely the formation of Klebanoff streaks in the boundary layer beneath free-stream forcing, their secondary instability and the onset of turbulence spots [4, 23]. Finally, we examine whether there is any evidence of the boundary layer relaxing to a nearly-separated state between impinging wakes.

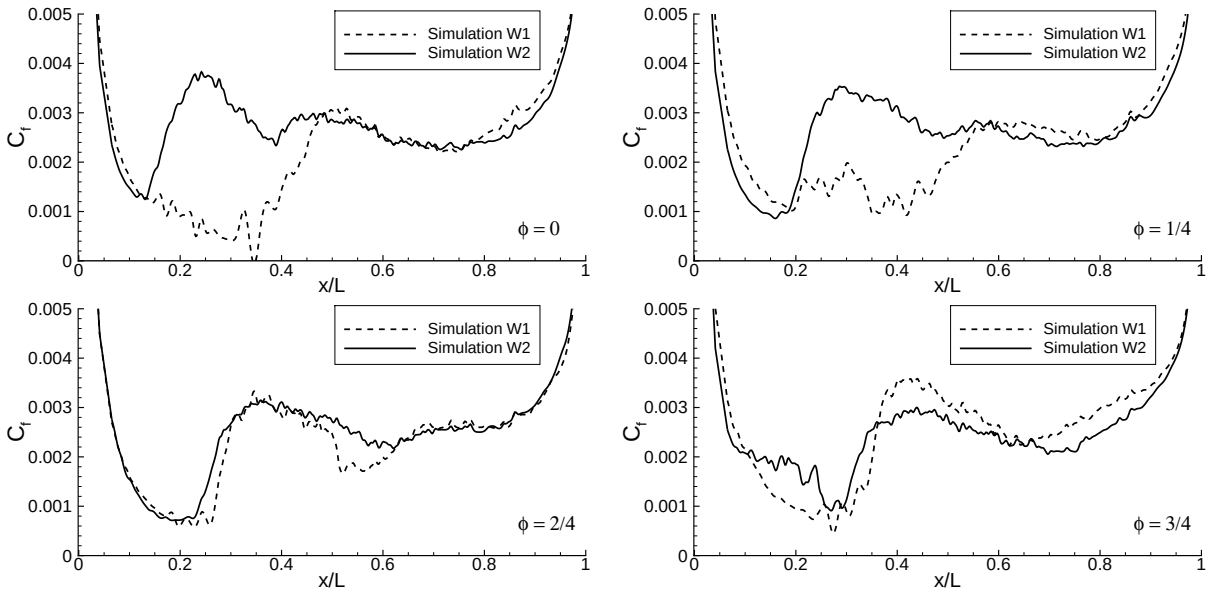

Figure 9: Phase-averaged friction coefficient along the pressure side from Simulations W1 and W2. The actual location of the wakes can be seen in Fig. 2

Figure 9 displays the phase-averaged skin friction, $\langle C_f \rangle$, along the pressure surface of the blade from simulations W1 and W2 at $\phi = \{0, 1/4, 2/4, 3/4\}$. As the wakes migrate along the surface of the blade, disturbances are introduced into the boundary layer. While in the absence of free-stream fluctuations the boundary layer on the pressure side was found to separate (see [27, 22]), in the presence of free-stream disturbances the boundary layer is likely to undergo transition to turbulence. The disturbances induced by the strong wakes (W2) are thereby expected to be more effective in triggering transition to turbulence - corresponding to a significant growth in the friction coefficient - relative to the weak wakes (W1). This is evident in the $\langle C_f \rangle$ curve at $\phi = 0$, where the strong wakes of simulation W2 manage to trigger transition between $x/L \approx 0.13$ and $x/L \approx 0.25$. The slight kink observed in $\langle C_f \rangle$ at $x/L \approx 0.38$ corresponds to an earlier transition event triggered by the preceeding wake. With the weaker wakes from simulation W1, transition occurs further downstream and is located between $x/L = 0.33$ and $x/L = 0.5$. Also, it can be seen that the pressure side boundary layer from W1 does indeed relax to a nearly separated state near $x/L = 0.35$. A further reduction of the wake-passing frequency and/or the wake-turbulence is likely to induce periodic separation and separation-induced transition.

At $\phi = 1/4$ the locations of transition in both simulations have moved with the wakes further downstream. The onset of transition in W2 has moved to $x/L \approx 0.17$. At the same location in W1, a slight increase in the phase-averaged skin friction can be observed. The distortion of the boundary layer, however, is not sufficient to cause a full transition to turbulence, which happens further downstream and is still associated with the preceeding wake.

At $\phi = 2/4$ transition in both simulations starts at $x/L \approx 0.25$ and ends at $x/L \approx 0.35$. The dips in the $\langle C_f \rangle$ signal near $x/L \approx 0.55$ again correspond to an earlier transition event. The sequence of snapshots in figure 9 give a clear evidence of the presence of a periodic transition scenario in both simulations triggered by the passing wakes. In general the strong wakes in simulation W2 introduce stronger disturbances into the pressure side boundary layer which trigger earlier transition at $\phi = 0$ and $\phi = 1/4$.

Finally, at $\phi = 3/4$ the onset of transition in both simulations has moved further downstream to $x/L \approx 0.27$, while transition ends at $x/L \approx 0.40$. In the simulation with strong wakes an incomplete transition event can be observed upstream, starting at $x/L \approx 0.10$.

The contour plots in figure 10 (upper part) identify the location of the maximum phase-averaged spanwise fluctuations, $\max_y \langle w_{rms} \rangle$ (corresponding to the maximum value of $\langle w_{rms} \rangle$ in the region between the wall and the edge of the boundary layer), in the pressure-surface boundary layer of simulations W1 (left) and W2 (right). The approximate path of the wakes along the edge of the boundary layer is identified by the dashed lines and the calmed region that forms in between impinging wakes is labelled "B". The figure shows that there is a correlation between the presence of the wake at the edge of the boundary layer and the presence of strong spanwise fluctuations inside the boundary

layer emerging after a slight phase-shift, $\Delta\phi \approx 0.3$. The observed phase shift is explained partially by the fact that the location of the wake is given at the edge of the boundary layer while the location of $\max_y \langle w_{rms} \rangle$ is well inside the boundary layer - the time lag is necessary for free-stream disturbances to penetrate the boundary layer and to trigger a response. Also, the propagation speed of disturbances inside the boundary layer is slower than that of the wake in the free stream. This is evidenced by the existence of an angle between the path of the wakes and the orientation of the contours - best visible in simulation W1 - immediately downstream of the leading edge. The white areas in between the paths of the wakes, upstream of $x/L \approx 0.5$, identify calmed regions in which the disturbance level inside the boundary layer is relatively low. Further downstream disturbances are present inside the boundary layer at all phases indicating that at these locations the boundary layer is fully turbulent. Compared to the weak-wake simulation W1 (left pane), the contours of simulation W2 (right pane) show a smaller calmed region and an earlier transition to turbulence. Compared to $\max_y \langle w_{rms} \rangle$, the maximum tangential fluctuations, $\max_y \langle u^t_{rms} \rangle$, show a similar pattern but with slightly smaller calmed regions in between the paths of the migrating wakes. The main differences are that the maxima of the streamwise fluctuations are located more upstream than the maxima in the spanwise fluctuations, and that the actual level of the streamwise disturbances is significantly higher. A possible explanation for the observed differences is that the periodic disturbances introduced in the boundary layer by the passing wakes trigger a Klebanoff distortion (streaks) which tends to lead to strong fluctuations in the streamwise direction and hence to a large $\max_y \langle u^t_{rms} \rangle$. Further downstream the streaks become unstable [17, 5] eventually leading to the observed amplification of $\max_y \langle w_{rms} \rangle$. The figure clearly demonstrates that both the appearence of streaks and the further transition to turbulence take place earlier in the strong wake simulation W2 relative to W1.

Figure 11 shows contours of the phase-averaged streamwise fluctuations along the pressure surface at phase $\phi = 7/8$. The snapshot contrasts the location of maximum $\langle u^t_{rms} \rangle$ within the pressure-surface boundary-layer to the location along the boundary-layer edge where the streamwise fluctuation level in the wake reaches its peak. This provides further evidence of the fact that the propagation speed of the wake-induced fluctuations inside the boundary layer is slower than the propagation speed of the wake in the free stream.

The four snapshots displayed in figure 12 show the time-evolution of contours of the tangential velocity fluctuations in a plane adjacent to the pressure surface. The plane in the background - that shows contours of the fluctuating velocity - identifies the location of the wakes. As the wake traverses the surface of the blade, the boundary layer is perturbed. As a result, immediately below the wake, high- and low-speed streaks appear in the boundary layer. At certain times, a patch of calmed flow can be observed in between the passing wake and the turbulent flow downstream (see snapshots at $t = 15.50\ L/U$ and $t = 15.75\ L/U$). The location of the onset of transition, associated with a passing wake, gradually moves downstream with the wake. Transition occurs when a number of turbulent spots appear almost simultaneously at a similar streamwise location. These spots grow in the downstream direction and eventually merge forming a fully-turbulent boundary layer.

Figure 13 shows contours of the spanwise velocity fluctuations and indicates where the streaks shown in figure 12 become unstable resulting in the development of local patches of turbulence. A one-to-one comparison of the snapshots in the two figures shows that the spanwise fluctuations first appear virtually at the same location as the first streaks. This evidences that when the wake triggers the formation of streaks in the pressure-surface boundary layer, it also introduces spanwise fluctuations. The latter contribute to streak instability and the onset of turbulence downstream.

4.2 The suction surface

Figure 14 shows a comparison of the phase-averaged friction coefficient, $\langle C_f \rangle$, along the suction surface from simulations W1 and W2. For all phases, the gradually decreasing $\langle C_f \rangle$ profiles upstream of $x/L = 0.4$ are identical. It should be noted that in the absence of free-stream disturbances, the entirely laminar flow along the suction side separates along a large portion of the blade [27, 22]. In that case the roll-up of the separated boundary layer resulted in the formation of strong two-dimensional KH rolls that convected downstream by the mean flow. In simulation W1, figure 14 shows that the boundary layer separates at all phases, as indicated by $\langle C_f \rangle$ becoming negative between $x/L \approx 0.45$ and $x/L \approx 0.50$. This is followed by a roll-up of the separated shear layer, which causes the significant oscillations in $\langle C_f \rangle$ downstream of $x/L = 0.55$.

Compared to simulation W1, the $\langle C_f \rangle$ signal in simulation W2 is significantly smoother. At the phases shown, only a small region of separation is identified as the separated boundary layer quickly undergoes transition to turbulence and reattaches. Only around $\phi = 5/8$ is separation of the time-averaged boundary layer entirely suppressed (see figure 15). Even though this suppression is only marginal (the minimum $\langle C_f \rangle$ value is virtually zero), it does show that the increased wake-strength in simulation W2 not only leads to a significant reduction in the phase-averaged size of the separation bubble for all phases but also periodically leads to a complete reattachment of boundary layer.

Figure 15 shows carpet plots of the maximum phase-averaged spanwise and streamwise fluctuations in the suction-side boundary layer as a function of phase. As indicated by figure 14, the boundary layer on the suction side tends to separate in both simulations. In the weak-wake case (W1) the size of the separation bubble is large and the weak wakes are ineffective in suppressing separation. Separation - indicated by the white contour line in the $\max_y\langle u^t_{rms}\rangle$ plot - occurs around $x/L = 0.46$. The contours of both the maximum spanwise and streamwise fluctuations show a sharp divide near $x/L = 0.6$. Upstream of this divide only periodic, wake-induced disturbances are seen to be present while downstream of this divide disturbances are present for all phases. When the wake reaches the region downstream of the divide, the local disturbances tend to grow, while in between wakes they slowly deminish. According to the time-averaged skin-friction shown in figure 6, reattachement of the time-averaged boundary layer takes place immediately downstream of the sharp divide, this is also evidenced by the downstream white contour line that oscillates near $x/L = 0.72$. The small islands of reattached flow near $\phi = \{0.2, 1.2\}$ and $x/L = 0.64$ most likely correspond to secondary separation inside the primary separation bubble - a similar observation was reported in the disturbance-free simulation [27, 22].

In the strong wake case (W2) the spanwise and streamwise fluctuations show a different pattern. It can be seen that separation is periodically suppressed fully and that (compared to W1) the separation line has moved downstream. The latter can be caused either by the streaks causing a mean flow distortion leading to a fuller boundary layer profile, or by the calming effect trailing the spots which prolonges the duration for separation to be re-established. In between the periodically passing wakes, the divide between the zones with and without boundary layer disturbances is no longer a straight line. Instead, after the wake passes, the divide gradually moves downstream indicating the presence of a calmed region. Boundary layer separation - again identified by the white contour in the $\max_y\langle u^t_{rms}\rangle$ plot - is periodically suppressed. The path of the wake along the edge of the boundary layer is identified by the dashed line. Every migrating wake introduces disturbances in the boundary layer somewhat upstream of separation. As the flow in the outer region of the boundary layer moves faster than near the wall, part of the disturbances are found inside the separated boundary layer on top of the separation bubble. At the same time, the slower moving near-wall region of the disturbed (non-separated) boundary layer upstream is locally becoming turbulent. When this fully turbulent patch moves downstream it is found to squash the separation bubble and both the spanwise and streamwise fluctuations are enhanced. Upstream of the separation bubble, the enhanced wake-induced streamwise fluctuations inside the boundary layer indicate that the wake manages to introduce Klebanoff modes (streaks) that, as also found by Coull and Hodson [3], first appear immediately downstream of the leading edge. The absence of large values of $\max_y\langle w_{rms}\rangle$, however, indicates that further transition to turbulence does not take place until after $x/L \approx 0.45$.

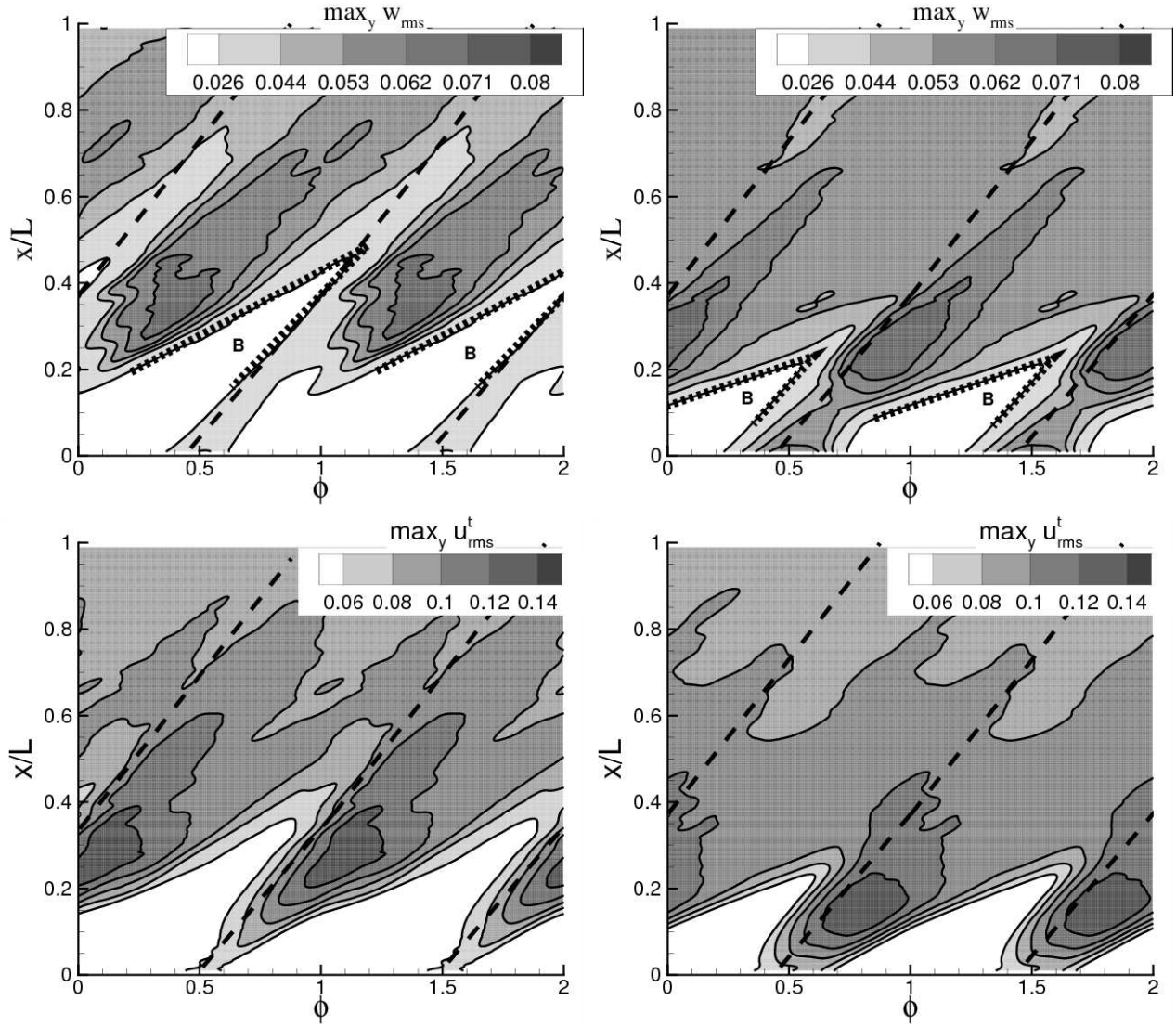

Figure 10: Contours of $\max_y \langle w_{rms} \rangle$ (upper part) and $\max_y \langle u^t_{rms} \rangle$ (lower part) along the pressure surface (carpet plots). Left: weak wakes, right: strong wakes. The location of the wakes at the edge of the boundary layer is identified by the dashed lines, The border of the becalmed region, labelled "B", is identified in the $\max_y \langle w_{rms} \rangle$ plots by the thick dotted lines.

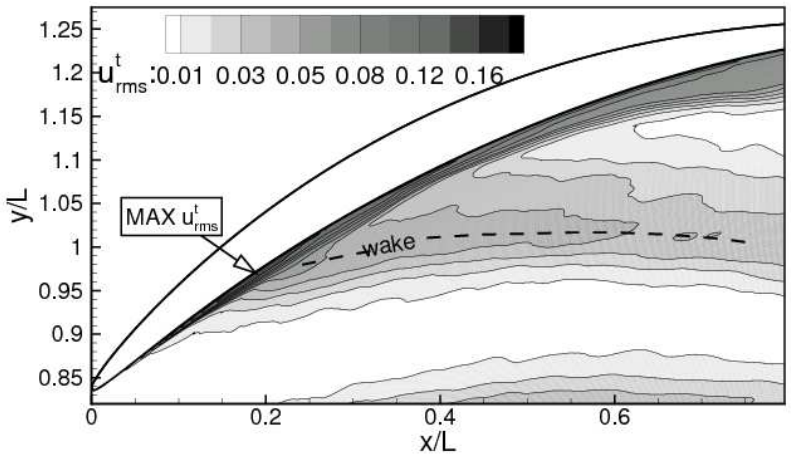

Figure 11: Simulation W2: Contours of $\langle u^t_{rms} \rangle$ along the pressure surface at $\phi = 7/8$.

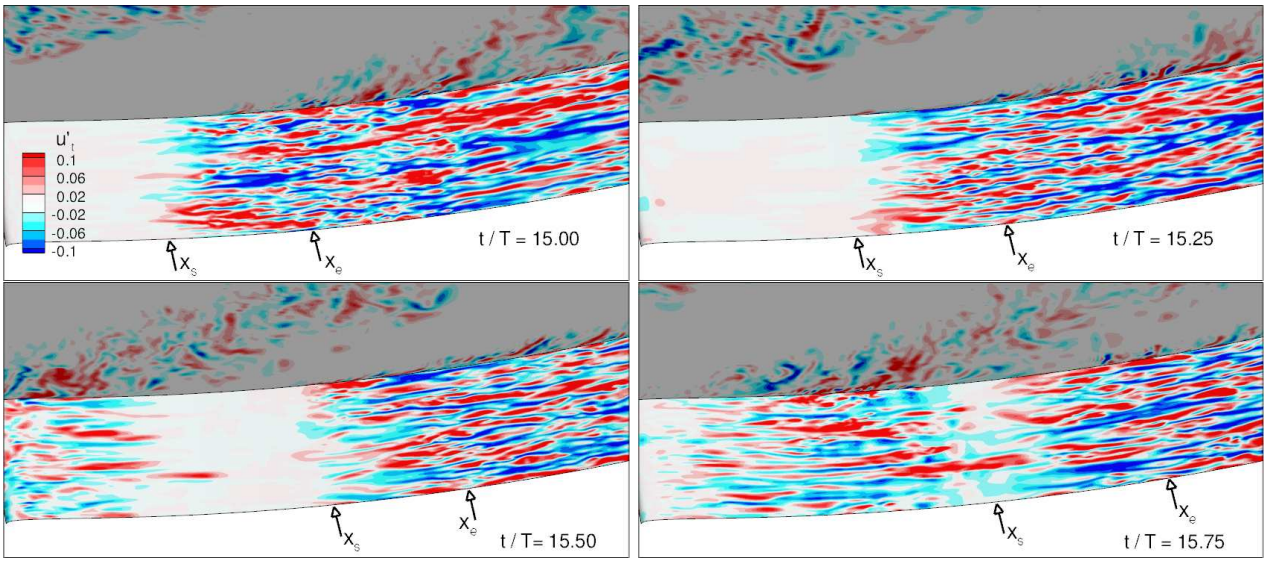

Figure 12: Simulation W2: Evolution of the tangential velocity fluctuations in a plane in the pressure side boundary layer at four different times. The plane at the back shows the spanwise velocity fluctuations to identify the location of the wakes. The arrows indicate the location of the start and end of transition as observed in the phase-averaged statistics, see also figure 9

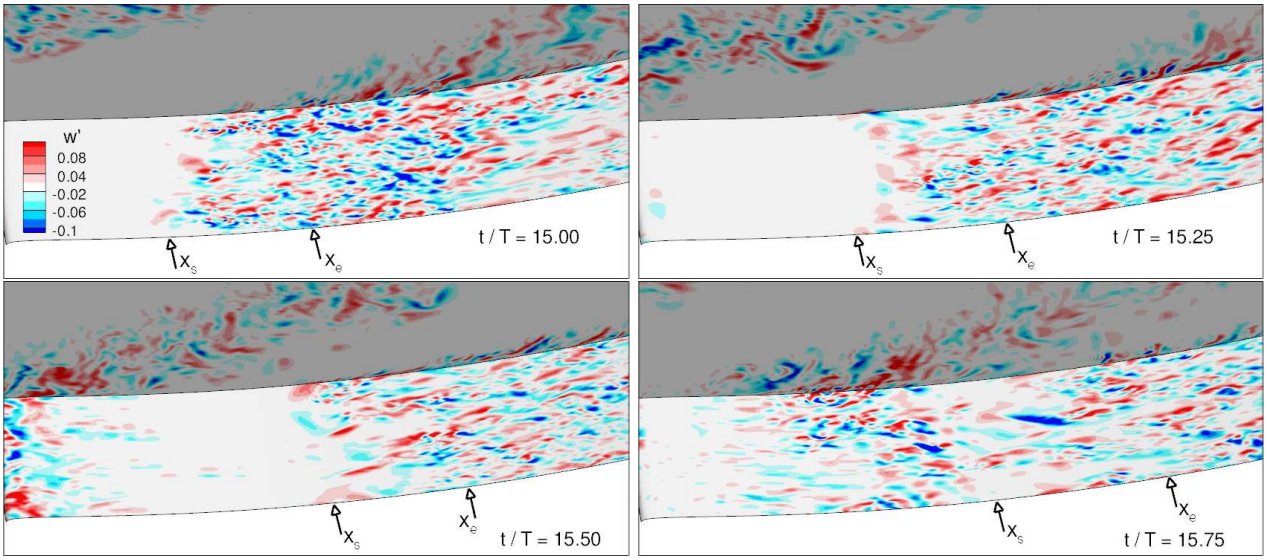

Figure 13: Simulation W2: Evolution of the spanwise velocity fluctuations in a plane in the pressure side boundary layer at four different times. The plane at the back shows the spanwise velocity fluctuations to identify the location of the wakes. The arrows indicate the location of the start and end of transition as observed in the phase-averaged statistics

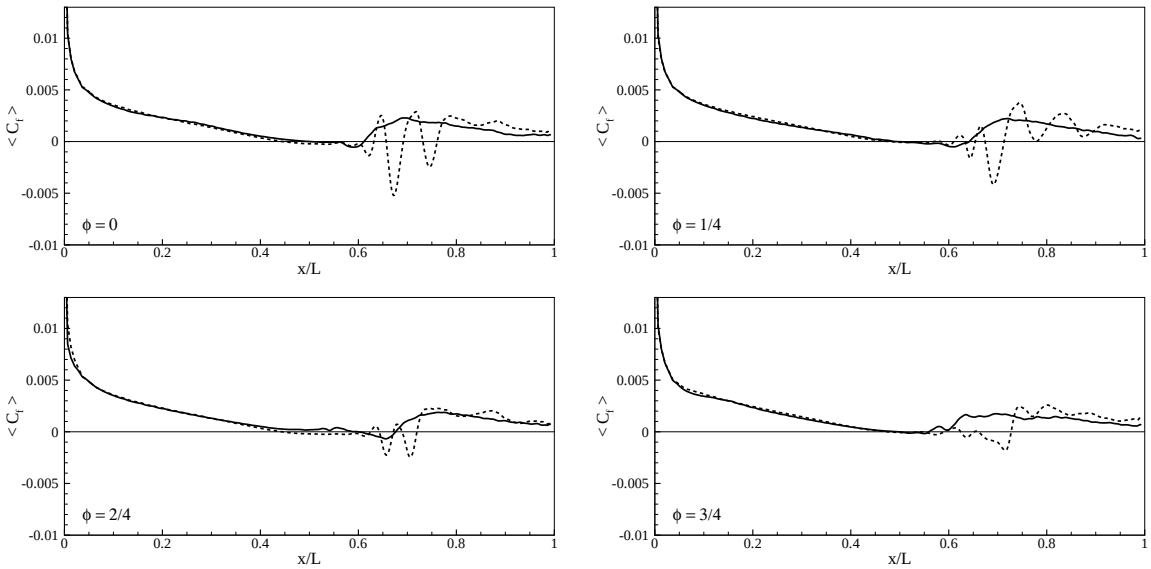

Figure 14: Phase-averaged friction coefficient $\langle C_f \rangle$ along the suction surface at phases $\phi = 0, 1/4, 2/4, 3/4$. Simulations W1 (- - -) and W2 (——)

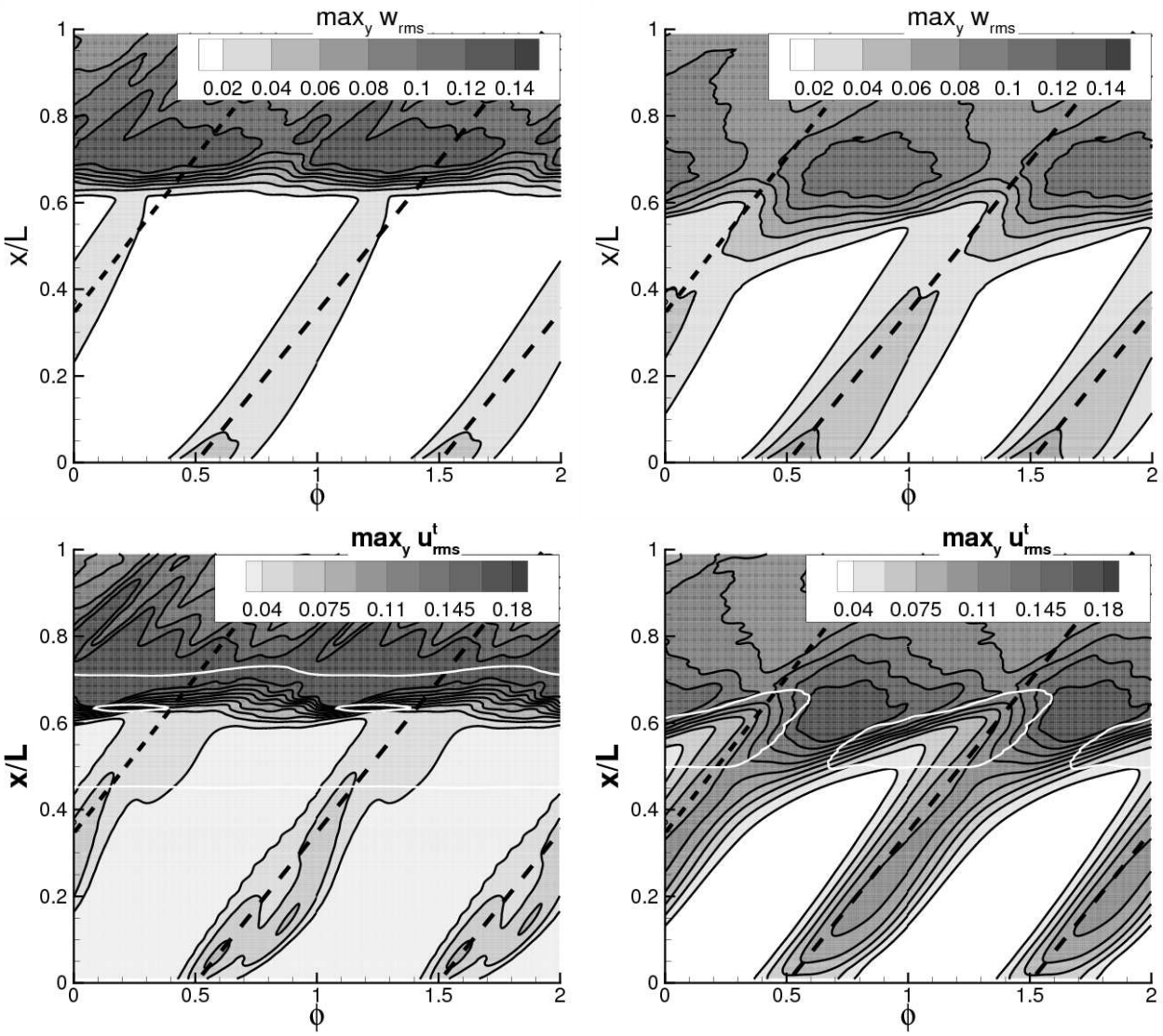

Figure 15: $\max_y\langle u^t_{rms}\rangle$ and $\langle w_{rms}\rangle$ along suction surface versus phase (carpet plot). Left: weak wakes (W1), right: strong wakes (W2). The white contour in the $\max_y\langle u^t_{rms}\rangle$ plots from simulations W1 & W2 identifies separation. As in figure 10, the dashed lines correspond to the location of the wakes at the edge of the boundary layer.

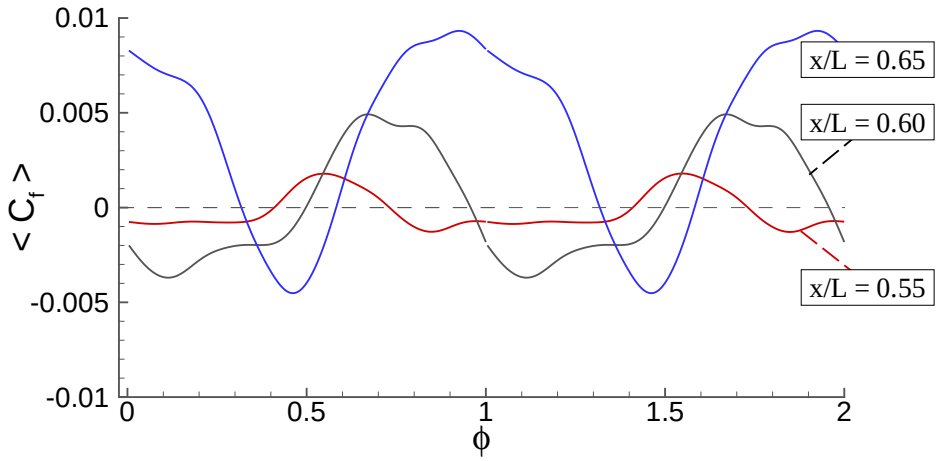

Figure 16: $\langle C_f \rangle$ versus phase at three locations along the suction surface from simulation W2

The phase-average friction coefficient is shown in figure 16 as a function of phase at three locations ($x/L = 0.55, 0.60, 0.65$) along the suction surface of the blade from simulation W2. As negative values of $\langle C_f \rangle$ correspond to flow separation, at $x/L = 0.55$ the boundary layer is separated 60% of the time. The periodic attachment (around $\varphi = 0.50, 1.50$) is directly related to turbulence induced inside the boundary layer by the wakes as they migrate through the passage between blades. Further downstream, the periodic reattachment takes place at a later phase and the period during which the flow remains attached is longer. At $x/L = 0.65$, for instance, the boundary layer is only separated 20% of the time. This increased duration of attachment might be related to turbulent spots spreading in the downstream direction and/or the calming effect caused by the turbulent nature of the attached upstream boundary layer profile. The fact that the maximum $\langle C_f \rangle$ increases in the downstream direction indicates that the turbulence in the boundary layer becomes more developed. At all locations, after the peak in the friction coefficient, the boundary layer slowly relaxes to a separated state, thus showing evidence of the "calming" which was also observed in the simulations with free-stream turbulence [27, 22]. The effect of turbulent spots generated upstream of separation is examined below.

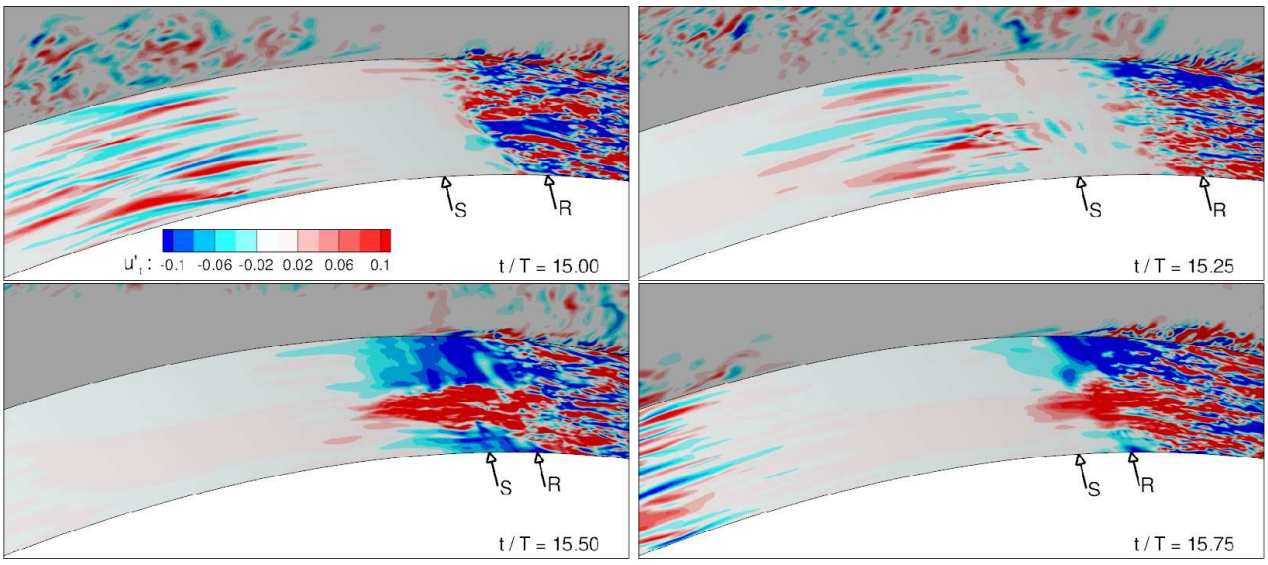

Figure 17: Simulation W2: Evolution of the tangential velocity fluctuations in a wall-parallel surface inside the suction side boundary layer at four different times. The plane at the back shows the spanwise velocity fluctuations to identify the location of the wakes. The arrows identify the locations of boundary layer separation (S) and reattachment (R).

The four snapshots shown in figure 17 illustrate the time-evolution of the fluctuating tangential velocity contours in a surface adjacent to the suction surface of the compressor blade. In the snapshots at $t = 15.00\ L/U$ and $t = 15.25\ L/U$, the streaks that are triggered inside the boundary layer by the fluctuations in the passing wake propagate much slower than the wake itself. At $t = 15.25\ L/U$, a turbulent spot is formed and quickly develops as it is convected downstream ($t = 15.50\ L/U$). As the flow is forced to intermittently reattach between $t = 15.50\ L/U$ and $t = 15.75\ L/U$, the distance between the phase-averaged locations of boundary layer separation ("S") and reattachment ("R") at these two instances becomes relatively small. In the absence of oncoming disturbances, the boundary layer slowly recovers to a laminar state eventually leading to an increase in size of the separation bubble.

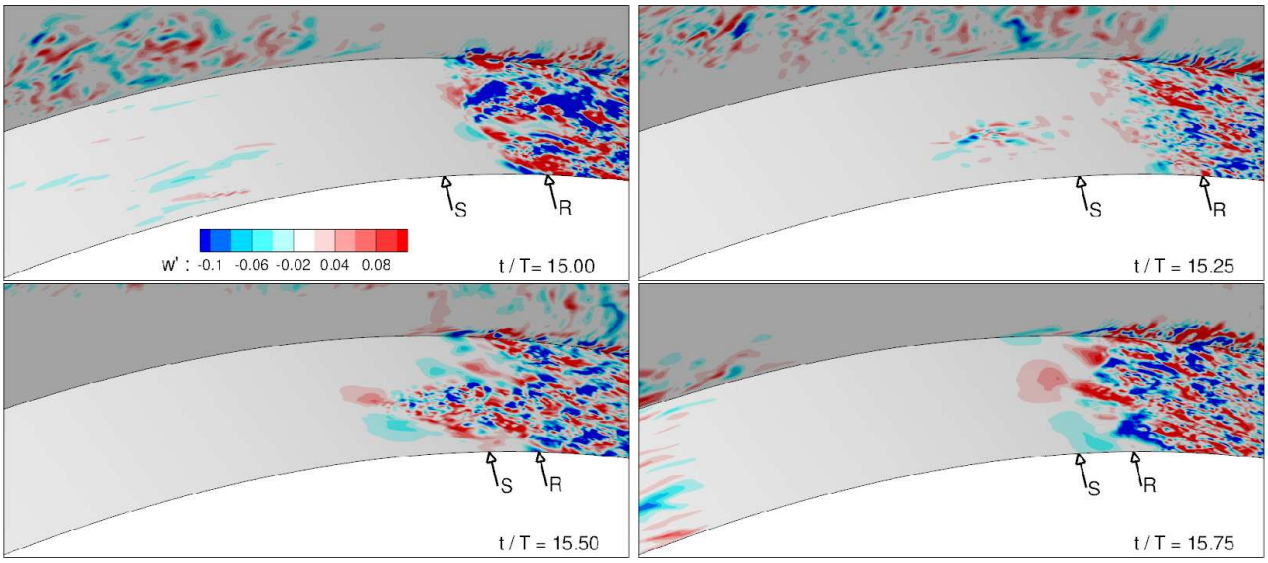

Figure 18: Simulation W2: Evolution of the spanwise velocity fluctuations in a plane in the suction side boundary layer at four different times. The plane at the back also shows the spanwise velocity fluctuations to identify the location of the wake, the arrows identify the phase-averaged locations of boundary layer separation (S) and reattachment (R).

Figure 18 shows the time-evolution of the spanwise fluctuations in a surface adjacent to the suction surface. As in figure 17, the contours of the fluctuating velocity in the back plane identify the location of the wakes. The streaks identified in figure 17 are observed to become unstable and develop localised pockets of increased spanwise fluctuations. In particular, the turbulent spots at $t = 15.25\ L/U$ and $t = 15.50\ L/U$ become clearly visible.

To illustrate the convection of the turbulent spot through the area where the boundary layer detaches, figure 19 shows a series of six snapshots of tangential velocity contours in a plane at a distance of $0.00089L$ from the suction surface. The location where the flow is separated is identified by the black line. The turbulent spot moves straight through the separated area causing a local reattachment of the boundary layer, while on both sides of the spot the boundary layer remains separated - as identified by the white areas.

An illustration of the interaction of the turbulent spot with the separation region is provided in figure 20. The figure shows the evolution of light isosurfaces of zero tangential velocity and dark isosurfaces - corresponding to a wall-normal velocity at $\pm 0.1\,U$ - which identify the shape and location of the turbulent spot. The front end of the spot is lifted up and moves downstream inside the detached boundary layer on top of the separated flow. The tail of the spot subsequently forces the flow to reattach as it impacts onto the separation bubble.

5 Discussion and Conclusions

The influence of periodically passing wakes on the boundary layer transition along a compressor blade was studied using direct numerical simulations of flow in a V103 compressor cascade. The incoming wakes were generated in a precursor simulation of flow around a circular cylinder at $Re_D = 3300$ in which snapshots of the instantaneous flow field were taken at a distance of $6D$ to the cylinder. Because of the proximity of the snapshots to the wake-generating cylinder, the incoming turbulent wakes still posess some of the characteristics of a von Karman vortex street and consisted of discrete patches of alternately rotating and counterrotating turbulent flow.

The effect of the strength of the wake on boundary-layer transition and boundary-layer separation was studied. On the pressure side, both the weak and strong wakes were found to trigger bypass transition of the boundary layer upstream of the location of separation identified in the disturbance-free simulation [27, 22]. As it passes over the blade, the strong wake induces transition shortly after the leading edge. The weaker wake causes transition further downstream. However, when the wakes have passed mid-chord, the two cases have almost the same skin friction curve and in that sense, transition is independent of wake strength at that phase (see fig. 9). This is so, despite the weak wake having a lower turbulent intensity. This implies that correlations between transition and free-stream turbulent intensity are not applicable to transition under passing wakes: the instantaneous intensity is not correlated with the instantaneous point of transition. The dynamics of the interaction between the wake and the boundary layer play a determinative role.

At some phases, the wakes introduced disturbances into the boundary layer relatively close to the leading edge. These disturbances, however, were damped while convecting downstream, resulting in a re-laminarization of the boundary layer. This was seen on both pressure and suction sides of the blade. Despite the adverse pressure gradient on the pressure side, disturbances decay near the leading edge. This argues against leading edge receptivity being the initial coupling between the disturbance and the boundary layer. The passing wake provides evidence that the coupling is locally to the downstream boundary layer. As they passed downstream, the boundary layer well upstream of the wakes returned to laminar. In the weak-wake simulation, the boundary layer in between two passing wakes was found to relax to a nearly separated state. The strong-wake simulation relaxed too, but did not show any sign of being close to separation. Transition originates just behind the wakes and is caused by local forcing. This substantiates the idea that bypass transition is a consequence of low-frequency modes that penetrate into the boundary layer [24, 26]. The consequent Klebanoff streaks are seen in the present simulations.

In the strong-wake-simulation it was found that separation on the suction surface was intermittently suppressed. In the weak-wake case the phase-averaged size of the suction-side separation bubble was only marginally affected by the actual location of the wake. As a result, transition to turbulence was found to take place in the separated shear layer and the location of transition was virtually independent of phase.

In the strong-wake simulation, the wakes introduced stronger disturbances in the suction side boundary layer, upstream of the location of separation. During each period, these disturbances were found to trigger streaks into the boundary layer which turned into turbulent spots as they were convected downstream. When reaching the location of separation, the head of the turbulent spot - which was slightly lifted up - moved into the separated boundary layer without causing it to reattach (figures 19 and 20). This caused a prompt, 3-dimensional breakdown of the separated shear layer. The flow underneath the spot was forced to locally reattach only when the tail of the spot reached the separation bubble.

Future work on DNS of flows in turbomachinery could include - the effect of periodic unsteadiness in the overall pressure gradient on boundary layer transition (this unsteadiness would be created by the movement of blades upstream of the passage), - simulation of more than one turbine/compressor passage, - simulation of a turbine/compressor passage with end-wall effects etc.

Simulation results can be made available on request.

Acknowledgements

The authors would like to acknowledge the steering committee of the Computing Centre (HLRS) of the University of Stuttgart for granting computing time on the NEC SX8.

References

[1] Breuer, M., Rodi, W.: Large eddy simulation for complex flow of practical interest. In: E.H. Hirschel (ed.) Flow simulation with high-performance computers II, Notes on Numerical Fluid Mechanics, volume 52. Vieweg Verlag, Braunschweig, Moscow: Nauka (1996)

[2] Cho, N.H., Liu, X., Rodi, W.: Calculation of wake-induced unsteady flow in a turbine cascade. ASME Paper 92-GT-306 (1992)

[3] Coull, J., Hodson, H.: Unsteady boundary-layer transition in low-pressure turbines. J. Fluid Mech. **681**, 370 – 410 (2011)

[4] Durbin, P.A., Wu, X.: Transition beneath vortical disturbances. Annual Review of Fluid Mechanics **39**, 107–128 (2007)

[5] Hack, M.J.P., Zaki, T.A.: Streak instabilities in boundary layers beneath free-stream turbulence. Journal of Fluid Mechanics **741**, 280–315 (2014)

[6] Hilgenfeld, L., Pfitzner, M.: Unsteady boundary layer development due to wake-passing effects on a highly loaded linear compressor cascade. J. Turbomachinery **126**, 493–500 (2004)

[7] Jacobs, R.G., Durbin, P.A.: Simulations of bypass transition. Journal of Fluid Mechanics **428**, 185–212 (2001)

[8] Kalitzin, G., Wu, X., Durbin, P.: DNS of fully turbulent flow in a LPT passage. Int. J. of Heat and Fluid Flow **24**, 636–644 (2003)

[9] Mayle, R.E.: The role of laminar-turbulent transition in gas turbine engines. ASME Paper 91-GT-261 (1991)

[10] Michelassi, V., Martelli, F., Dénos, T., Arts, T., Sieverding, C.: Unsteady heat transfer in stator-rotor interaction by two-equation turbulence model. ASME J. Turbomachinery **121**, 436 – 447 (1999)

[11] Nagarajan, S., Lele, S., Ferziger, J.: Leading edge effects in bypass transition. Journal of Fluid Mechanics (2007)

[12] Nolan, K.P., Zaki, T.A.: Conditional sampling of transitional boundary layers in pressure gradients. Journal of Fluid Mechanics **728**, 306–339 (2013)

[13] Rhie, C., Chow, W.: Numerical study of the turbulent flow past an airfoil with trailing edge separation. AIAA. J. **21**(11), 1525–1532 (1983)

[14] Stadtmüller, P., Fottner, L.: A test case for the numerical investigation of wake-passing effects of a highly-loaded lp turbine cascade blade. ASME paper 2001-GT-311 (2001)

[15] Stieger, R., Hodson, H.: Convection of a turbulent bar wake through a low-pressure turbine cascade. ASME J. Turbomachinery **127**, 388 – 394 (2005)

[16] Stone, H.: Iterative solutions of implicit approximations of multidimensional partial differential equations. SIAM. J. Nunerical Analysis **5**, 87–113 (1968)

[17] Vaughan, N.J., Zaki, T.A.: Stability of zero-pressure-gradient boundary layer distorted by unsteady klebanoff streaks. Journal of Fluid Mechanics **681**, 116–153 (2011)

[18] Wissink, J.: DNS of separating low Reynolds number flow in a turbine cascade with incoming wakes. Int. J. of Heat and Fluid Flow **24**, 626–635 (2003)

[19] Wissink, J., Rodi, W.: Numerical study of the near wake of a circular cylinder. Int. J. of Heat and Fluid Flow **29**, 1060–1070 (2008)

[20] Wissink, J., Rodi, W., Hodson, H.: The influence of disturbances carried by periodically incoming wakes on the separating flow around a turbine blade. Int. J. of Heat and Fluid Flow **27**, 721–729 (2006)

[21] Wu, X., Durbin, P.A.: Existence of longitudinal vortices evolved from distorted wakes in a turbine passage. Journal of Fluid Mechanics **446**, 199–228 (2001)

[22] Zaki, T., Wissink, J., Durbin, P., Rodi, W.: Direct numerical simulations of transition in a compressor cascade: the influence of free-stream turbulence. J. Fluid Mechanics **665**, 57–98 (2010)

[23] Zaki, T.A.: From streaks to spots and on to turbulence: Exploring the dynamics of boundary layer transition. Flow, Turbulence and Combustion **91**, 451–473 (2013)

[24] Zaki, T.A., Durbin, P.A.: Mode interaction and the bypass route to transition. Journal of Fluid Mechanics **531**, 85–111 (2005)

[25] Zaki, T.A., Durbin, P.A.: Continuous mode transition and the effects of pressure gradient. Journal of Fluid Mechanics **563**, 357 – 388 (2006)

[26] Zaki, T.A., Saha, S.: On shear sheltering and the structure of vortical modes in single- and two-fluid boundary layers. Journal of Fluid Mechanics **626**, 111–147 (2009)

[27] Zaki, T.A., Wissink, J.G., Durbin, P.A., Rodi, W.: Direct computations of boundary layers distorted by migrating wakes in a linear compressor cascade. Flow, Turbulence and Combustion **83**(3), 307–322 (2009)

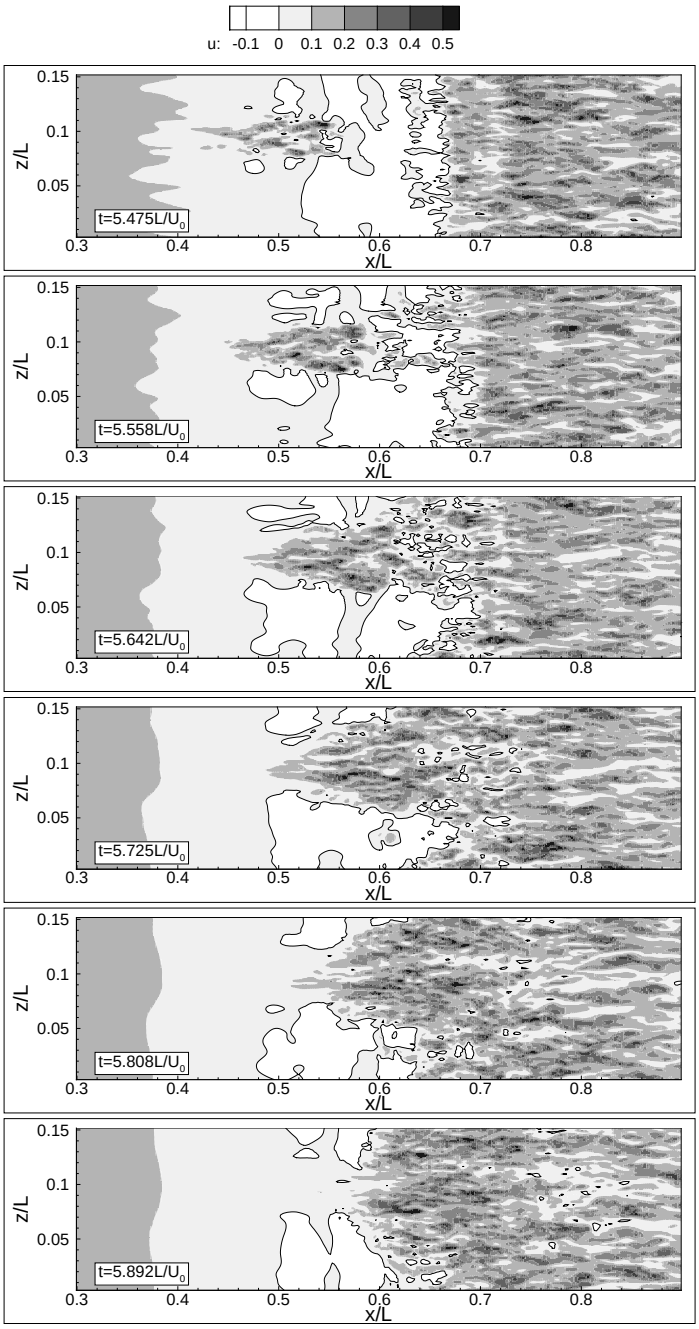

Figure 19: Simulation W2: A sequence of snapshots showing the evolution a turbulent spot as it is convected through a separation bubble in simulation W2. The figures shows contours of the tangential velocity in a surface at a distance $0.00089L$ from the suction surface. The black curve identifies the region where the flow is separated

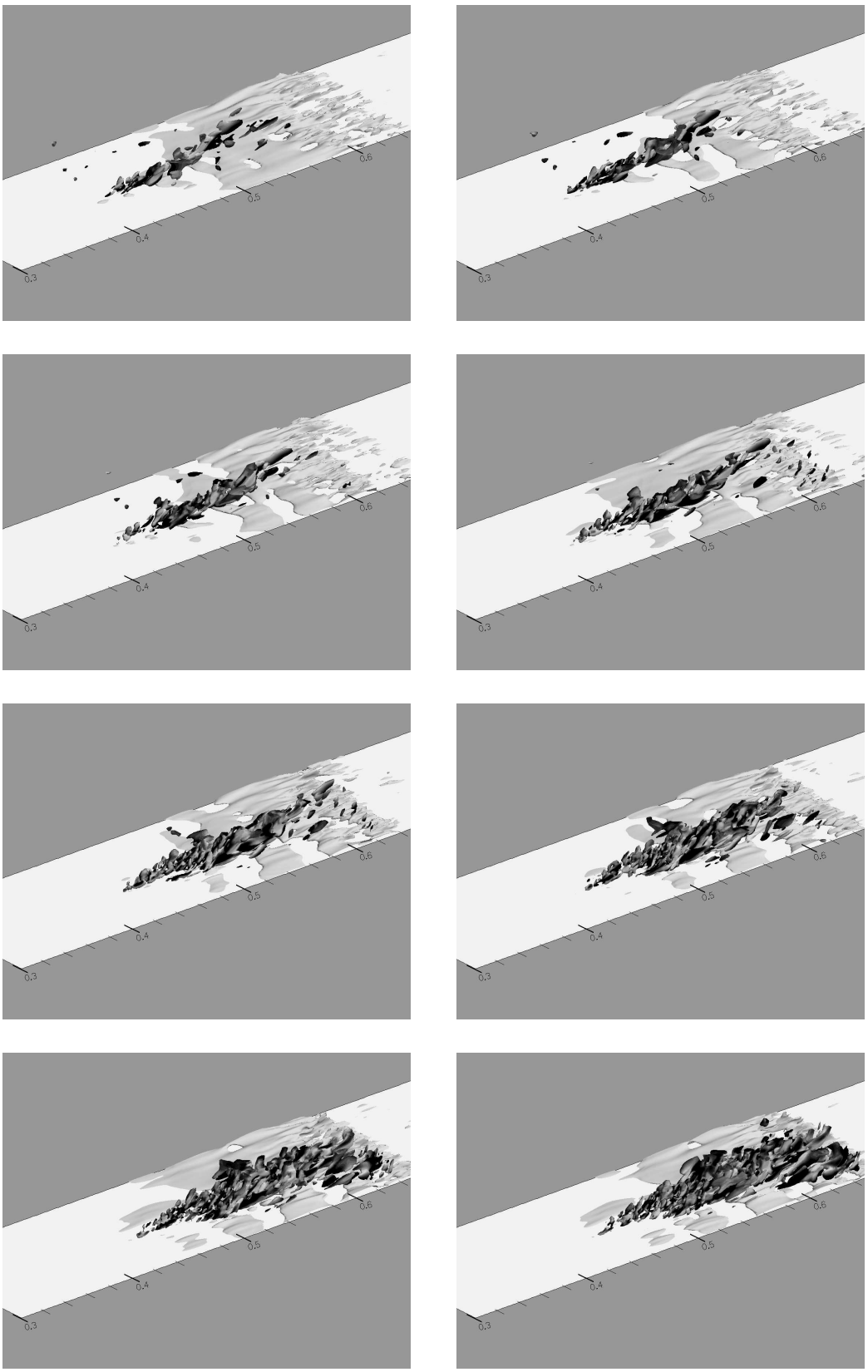

Figure 20: Simulation W2: A sequence of snapshots illustrating the movement of a turbulent spot (dark isosurfaces) through a separation bubble (light isosurface). The dark isosurfaces correspond to a wall-normal velocity of $\pm 0.1\,U$ and the light-gray isosurface corresponds to zero tangential velocity.